Halide Electroadsorption on Single Crystal Surfaces

B.M. Ocko* and Th. Wandlowski**
* Department of Physics, Brookhaven National Laboratory, Upton, N.Y. 11973
** Department of Electrochemistry, University of Ulm, D-89069, Ulm, Germany

ABSTRACT

The structure and phase behavior of halides have been investigated on single crystals of Ag and Au using synchrotron x-ray scattering techniques. The adlayer coverages are potential dependent. For all halides studied we found that with increasing potential, at a critical potential, a disordered adlayer transforms into an ordered structure. Often these ordered phases are incommensurate and exhibit potential-dependent lateral separations (electrocompression). We have analyzed the electrocompression in terms of a model which includes lateral interactions and partial charge. A continuous compression is not observed for Br on Ag(100). Rather, we find that the adsorption is site-specific (lattice gas) in both the ordered and disordered phases. The coverage increases with increasing potential and at a critical potential the disordered phase transforms to a well-ordered commensurate structure.

INTRODUCTION

A true atomistic picture of the electrode interface is emerging. This development is primarily due to the introduction of *in-situ* structural methods, specifically, scanning tunneling microscopy (STM), atomic force microscopy (AFM), and X-ray techniques, including surface X-ray scattering (SXS). Studies using these techniques have shown that electrode surfaces are often very well ordered and that the sharp features observed using classical electrochemical techniques are correlated with adlayer and substrate surface phase transitions. Due to the inherently high spatial resolution of SXS, the incommensurate structures can be measured with high precision. thus permitting small potential dependent changes to be determined. Additional information is obtained by investigating the potential dependence of the scattering amplitudes.

Here we review recent SXS results of halide adsorption on the (111) and (100) faces of Au and Ag. There are several reviews of SXS studies of electrode surfaces which will guide the curious reader[1-5]. SXS studies of electrode surfaces have revealed that electrodeposited adlayers (metals and halides) may be either commensurate, uniaxially incommensurate, or biaxially incommensurate with the underlying substrate.

RESULTS

An important finding of the present work is that the incommensurate phases are electrocompressive, that is, the distances between the neighboring atoms depend on the applied electrochemical potential. In Fig. 1 simple atomic models corresponding to these three structures on a (111) surface, hexagonally closed packed, are shown. Both panels B and C are incommensurate and electrocompressive. In panel A the adlayer is hexagonal, $(\sqrt{3} \times \sqrt{3})R30°$, where the atomic distance are $\sqrt{3}$ larger and the adlayer is rotated by 30° with respect to the underlying lattice. In panel B the adlayer is uniaxial-incommensurate, rectangular $c(p \times \sqrt{3})$, two atoms per unit cell, where the cell has dimensions of p and $\sqrt{3}$. In panel C the adlayer structure is incommensurate rotated-hexagonal. In a SXS experiment, the symmetry is uniquely determined by the characteristic diffraction pattern. Furthermore, the atomic distances can be determined to better than 0.01Å by the positions

Mat. Res. Soc. Symp. Proc. Vol. 451 © 1997 Materials Research Society

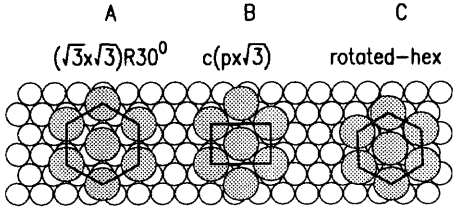

Figure 1: Atomic model of halide structures for (111) facets. These structures are (A) commensurate, (B) the uniaxial-incommensurate, and (C) rotated-hexagonal.

of the diffraction peaks in reciprocal space. The coverage, θ, relative to the number of atoms in a underlying metal layer, is directly calculated from the distances and symmetry. The adsorption of halides can be monitored using impedance measurements, chronocoulometry and cyclic voltammetry (CV). The initial adsorption typically gives rise to a broad peak in the CV which is often followed by several sharp peaks at higher potentials[6-10]. The first sharp peak in the CV usually corresponds to a transition from a disordered adlayer to an ordered adlayer. The additional peaks correspond to transitions between different ordered structures. All of the ordered halide adlayers form over a potential regime where the the underlying silver and gold lattices are unreconstructed[11]. In this report all potentials are referenced to a Ag/AgCl(3M NaCl) reference electrode.

A. Iodide on Ag(111) and Au(111)

In the first example we consider the adsorption of iodide on the (111) faces of Au and Ag. Iodine is the largest, most polarizable, and strongest adsorbing of the halides and exhibits ordered phases over the widest potential region. Since silver and gold have nearly identical lattice constants, a comparison of the iodide phase behavior allows us to focus on the relative role of the substrate-halide interaction. The Ag(111) surface is hexagonal, see open circles in Fig. 1., with a silver-silver nearest neighbor separation, $a_{Ag} = 2.889$Å. With increasing potential, the adsorption of iodide on Ag(111) gives rise to the series of three ordered structures shown in Fig. 1[14]. The coverage extends from exactly 1/3 in the commensurate phase to 0.442 at the most positive potentials. In Fig. 2 the potential dependent iodide coverage on the Ag(111) surface is shown in 0.1 M NaI as open circles. The commensurate phase is stable from about -0.9 to -0.94 V. No ordered iodide phase is observed below -1.0 V. The $c(p \times \sqrt{3})$ incommensurate phase exists between -0.92 to -0.36 V. Here θ continuously increases from about 0.355 to 0.40. At the most positive extreme of the $c(p \times \sqrt{3})$ phase, the structure corresponds to the $(5 \times \sqrt{3})$ high-order commensurate unit cell with a nearest-neighbor iodide spacing of 4.39 Å. Upon a slight further increase in potential, the $(5 \times \sqrt{3})$ phase vanishes and a rotated-hexagonal phase forms with $\theta = 0.417$ corresponding to $a_I = 4.59$ Å.

We now contrast the phase behavior of I on Ag(111) with that on Au(111)[10] in 0.1 M KI, shown in Fig. 2 as filled circles, where the gold lattice constant, $a_{Au} = 2.885$ Å is slightly smaller than a_{Ag}. The commensurate phase is never observed on Au(111), rather it is intercepted by the disordered (fluid) phase at the potentials where it would be expected. As demonstrated in Fig. 2, similar phase behavior on the two metals is observed in the $c(p \times \sqrt{3})$

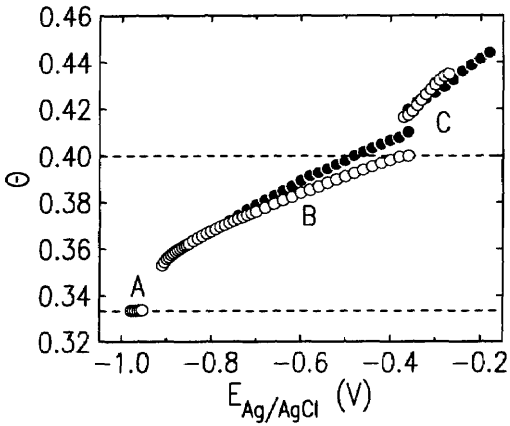

Figure 2: The potential dependent coverages, θ, of iodide, determined from the in-plane diffraction, are shown versus the applied potential on Ag(111) in 0.1M NaI as open circles and on Au(111) in 0.1 M KI as filled circles. The potential scale of the Au(111) data has been shifted negatively by 0.5 V to facilitate the comparison with the Ag(111) data.

and the rotated-hexagonal phases. In the $c(p \times \sqrt{3})$ phase the maximum coverage and the electrocompressibility, $d\theta/dE$ are slightly smaller on silver than gold. Almost identical behavior is observed in the rotated-hexagonal phase which suggests that the influence of the substrate is minimal within this phase.

Many aspects of the observed phase behavior can be understood in terms of the adjustable electrochemical potential which favors increased surface densities at higher potentials, and the competition between the adsorbate-adsorbate interaction and the adsorbate-substrate interaction. In the uniaxial-incommensurate phase the adsorbates reside between the rows of the substrate atoms and this configuration has a lower interfacial energy than the rotated-hexagonal phase where some of the adsorbates must be in high energy atop sites. However, the uniaxial-incommensurate phase is slightly distorted from the hexagonal configuration and this distortion increases the adsorbate-adsorbate elastic interaction energy. With increasing potential the distortion increases and at a critical potential the uniaxial-incommensurate phase transforms to the incommensurate, rotated-hexagonal phase.

B. A Comparison of Chloride, Bromide and Iodide Monolayers on Au(111)

Incommensurate, hexagonal monolayers are observed for chloride[12], bromide[13], and iodide[10] on the Au(111) electrode prior to bulk electrooxidation. Whereas the bromide and iodide monolayers are rotated by several degrees with respect to the Au(111) axis, the chloride monolayer is aligned. In Fig.3 the halide-halide separations are shown for the three halides in their incommensurate hexagonal phases. With increasing potentials the separations decrease; saturation is evident for bromide at the highest potentials, $\approx 0.7V$. The chloride-chloride separation ranges from 3.98-4.03 Å, the bromide-bromide separation ranges from 4.03-4.22 Å, and the iodide-iodide separation ranges from 4.46-4.33 Å. These difference reflect the different intrinsic sizes of the three atoms. For all three the minimum

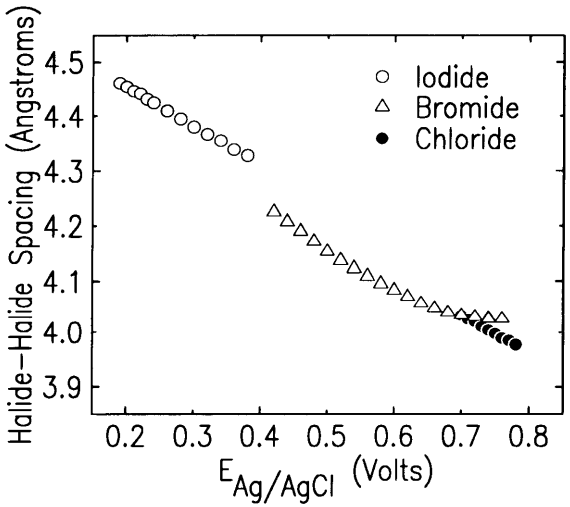

Figure 3: Comparison of halide-halide separations for chloride (0.1 M NaCl), bromide (0.1 M NaBr), and iodide (0.1 M KI) on Au(111).

spacings are close to the Van der Waals diameters and the maximum spacings are about 6% larger than that of the minimum. Despite the different intrinsic sizes of the halides and the potential range of the ordered hexagonal structures, the respective slopes, $\partial\theta/\partial E$ are very close for all three[12]. Quantitatively, the measured electrocompressibilities are $\partial\Gamma/\partial E$ are 2.41 $\pm$0.15, 2.95 $\pm$0.07, and 1.98 $\pm$0.02 ($10^{14} cm^2/V$) for chloride, bromide, and iodide, respectively, where $\Gamma = \theta/A_{Au}$ is the absolute coverage and A_{Au} is the area per underlying gold atom. The similar slopes imply that the repulsive lateral interactions for all three halides are comparable and suggests that the fundamental nature of the repulsive interactions are similar despite the different partial charge of these species. Analysis of the electrocompression in terms of specific lateral interaction models is presented below.

C. Bromide on Au(100)

How does the substrate structure affect the structure and coverage of the adsorbate? In order to explore this issue, we have carried out studies of the electrodeposition of Br on the Au(100) surface[15]. As shown in Fig. 4 by the open circles, this surface has an underlying square symmetry. Since the nearest-neighbor Au-Au separation is spacing of 2.885 Å this gives 1.20×10^{15} gold atoms/cm^2 corresponding to 86.6% of the Au(111) density. In bromide containing solutions, we find at lower potentials a commensurate $c(\sqrt{2}\times 2\sqrt{2})R45°$ phase (see Fig. 4 A) with $\theta = 1/2$. This commensurate structure contains two atoms in a rectangular unit cell with sides 4.08Å and 8.16Å. By construction, the nearest-neighbor separations are 4.08Å and 4.56Å. This phase is unusual since the atoms reside on bridge sites rather than the more coordinated four-fold hollows sites. The latter coordination is found for the $(\sqrt{2} \times \sqrt{2})R45°$ phase, often referred to as $c(2 \times 2)$, which also has $\theta = 1/2$ and is more commonly observed on fcc (100) surfaces (see Fig. 4C). However, the symmetry of this

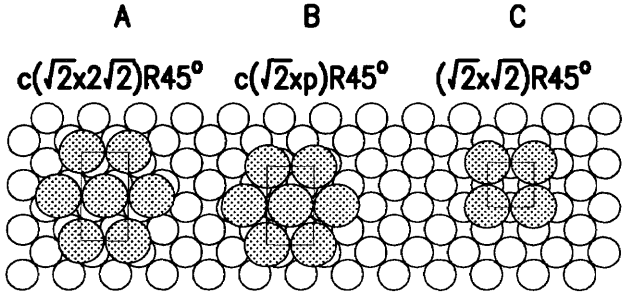

Figure 4: Atomic model of halide structures for (100) facets. These structures are (A) commensurate, (B) the uniaxial-incommensurate, and (C) commensurate.

phase is square whereas the $c(\sqrt{2} \times 2\sqrt{2})R45°$ phase is closer to hexagonal. The preference for the $c(\sqrt{2} \times 2\sqrt{2})R45°$ phase suggests that the elastic interactions between the relatively large Br adsorbates, which favor hexagonal packing, are more significant than the adsorbate-substrate interaction energy difference between the two phases. Above 0.42 V in 0.05 NaBr, the $c(\sqrt{2} \times 2\sqrt{2})R45°$ transforms to a uniaxial-incommensurate $c(\sqrt{2} \times p)R45°$ as shown in Fig. 4B, where $p = \frac{\sqrt{2}}{1+\epsilon}$ and ϵ is a measure of the incommensurability and varies continuously between 0 and 0.12 over the potential range 0.42 to 0.60 V, respectively. The potential dependent bromide coverage Γ, shown as circles in Fig. 5, is proportional to $1 + \epsilon$. Whereas the nearest-neighbor distance is always 4.08Å, the next-nearest-neighbor spacing decreases from 4.56Å for $\epsilon = 0$ (commensurate) to 4.13Å when $\epsilon = 0.12$. Thus the distortion from hexagonal symmetry, determined from the ratio between the nearest-neighbor and next-nearest-neighbor distances, decreases from 11.7 % to 1.2 % over the measured range. Despite the small distortion at this potential, the coverage at 0.60 V on the Au(111) face is still 3% higher than on the (100) face. The positive potential ranges are limited by the stability of the gold with respect to Br induced corrosion. Consequently, the more densely packed (111) face is more stable than the more open (100) face and the (111) data extends to higher potentials. The absence of satellite peaks for Br on Au(100), within the limits of the diffuse scattering background, allows us to establish that the compression is nearly uniform and not a network of locally commensurate regions separated by domain walls. The coverage in the neighborhood of the commensurate-incommensurate transition varies continuously. Accordingly, this transition is a second order phase transition. The measured critical exponent, β, which describes the behavior of incommensurability versus the potential, has been obtained by fitting the incommensurability to the form $\epsilon = (E - E_0)^\beta$ in the incommensurate phase. When the entire range is used in the fitting $\beta = 0.4 \pm 0.04$, however systematic deviations from this form are evident. Over a range restricted to $\epsilon < 0.06$ the data is consistent with $\beta = 1/2$. The dependence of β on the range is a direct consequence of the saturation which occur at the most positive potentials.

Over a range of coverages, between about 6.45×10^{14} to $6.70 \times 10^{14} cm^{-2}$, the close-packed Br monolayers on Au(100) and Au(111) exhibit similar electrocompressibilities, albeit a potential shift of 0.1 V. The similarity in the potential dependences, despite the uniaxial-compression on Au(100) compared to the biaxial compression on Au(111), suggests that the

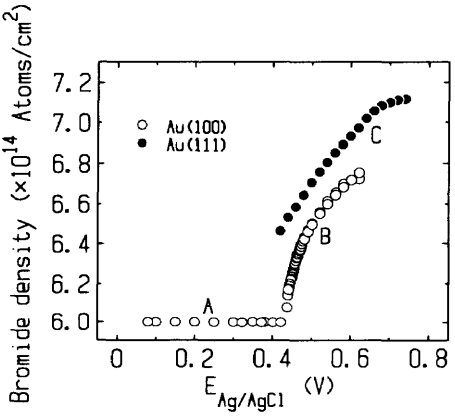

Figure 5: The potential dependent bromide coverages, Γ, in units of $atoms/cm^2$, on Au(100) and Au(111), determined from the in-plane diffraction, are shown versus the applied potential. The letters A,B and C in the figure refer to the structures given in Fig. 4. The Au(100) and Au(111) studies were carried out in 0.05 M NaBr and 0.10 M NaBr solutions, respectively. This concentration difference causes a +0.018 V shift for the Au(111) data set.

interactions between the Au and Br are similar in both cases and that the symmetry of the substrate does not play a critical role.

D. Bromide on Ag(100)

For bromide on Ag(100) a $(\sqrt{2} \times \sqrt{2})R45°$ structure with $\theta = 1/2$ is formed[16] (see Fig. 4C) where the bromides reside in the four-fold hollows. This square diffraction pattern is identical to the pattern observed for vapor deposited Cl on Ag(100) using LEED[17]. The neighboring bromides are 4.086Å apart and the coverage $\theta = 0.5$. Below a critical potential only the integer diffraction peaks associated with a (1×1) unit cell are observed. Half-order peaks, identifying the $(\sqrt{2} \times \sqrt{2})R45°$ phase, are observed above this critical potential. No incommensurate phases, such as observed for Br on Au(100)[15] is observed. The square packing arrangement of the adsorbed Br adlayer represents a large distortion from hexagonal packing. Furthermore, this arrangement is very different from the hexagonal packing formed on Ag(111)[14] and Au(111)[12], and the distorted-hexagonal pattern formed on Au(001). Electrodeposited chloride and iodide on Ag(100) exhibit the same diffraction features as that of bromide, thus they form the same c(2x2) phase without regard to the different halide diameters. In contrast, these same halides exhibit very different distances of closest approach on Au(111)[12].

In Fig. 6 the cyclic voltammetry (CV) and the potential dependent x-ray scattering intensity at (1/2,1/2,0.12) and at (1,0,0.12) are shown during both sweep directions (primitive lattice coordinates). The broad weak peak in the CV at about -1.1 V has been historically attributed to the reorientation of surface water and the second, sharper peak at about (-0.75 V) to a phase transition in the adsorbate layer[18]. On the basis of the potential dependent scattering at the half-order positions and no other identifiable features below this potential,

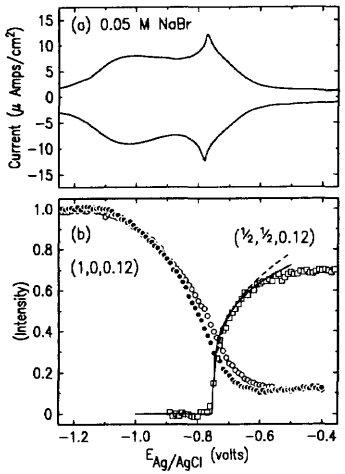

Figure 6: Comparison of the electrochemical and X-ray scans from the Ag(100) surface in 0.05 M NaBr. The cyclic voltammogram (10 mV/sec.) is shown in (a) has been obtained using a separate cell. The diffracted x-ray signals (1 mV/sec.) at (0.5,0.5,0.12) and (1,0,0.12) are shown in (b). Both intensities are normalized such that the intensity at (1,0,0.12) at -1.2 V are unity.

we identify the sharp peak as an order/disorder transition. At potentials more positive than -0.78 V the scattering intensity, after correcting for the diffuse component, starts to rapidly increase from zero as demonstrated by the data at (1/2,1/2,0.12) shown as squares in Fig. 1b. This result clearly identifies the sharp peak in the CV with the ordered phase. Saturation occurs at about -0.5V, corresponding to the potential where the CV saturates.

The x-ray intensity at superlattice positions, such as (1/2,1/2), measures the order parameter squared and is isomorphic to the magnetization in the Ising spin problem. Thus, the intensity should behave as $(E - E_c)^{2\beta}$ for $E > E_c$ $\beta = 1/8$. This prediction, shown as the solid line in Fig. 3 for the negative potential sweep, provides a reasonable description of the critical behavior up to about 80% of the saturation value. The fit for the other sweep direction is similar, except for an offset of 30 mV (see Fig. 6). This may be due to the fact that the transition is slightly first order or to slight changes in the surface morphology with sample history. Clearly, the mean-field prediction ($\beta = 1/2$) does not provide a reasonable description of the critical behavior. For Cl on Ag(100) in UHV[17], $\beta = 0.12 \pm 0.04$, however in this study the chemical potential was not directly measured but rather it was ascertained from the coverage.

The nature of the disordered phase is revealed by considering the potential dependent scattering intensity at (1,0,0.12), see Fig. 6, which is sensitive to both the arrangement of the surface silver atoms and that of the adsorbate layer. The onset of the slow decrease with increasing potential initiates at about -1.0 V and is correlated with the broad peak in the CV but occurs after the initial increase in the current (e.g adsorption). Close to the potential where long range order in the bromide monolayer is established there is a slight increase in

the magnitude of the slope in the intensity at (1,0,0.12) but no discontinuity. This indicates that the coverage changes continuously and supports the notion that the phase transition is close to being second order. At the most positive potentials, where the ordered phase is well developed, the intensity has reached a ratio which is 11% of its value in the absence of bromide. This ratio is in perfect agreement with crystallographic calculations which take into account the Ag(100) structure, the Br adlayer structure, and the relative scattering amplitudes of Ag and Br. The continuous decrease in the scattering intensity at (1,0,0.12) results from a continuous increase in coverage from zero to one half. On this basis, we assert that the disordered phase is a "lattice-gas" corresponding to random bromide adsorbed on four-fold hollow sites. Here we note that for Br on Au(111) and Au(100) there is no corresponding interference of the bromide scattering with that of the underlying lattice, as such, there is no evidence that these systems form a lattice gas. An analysis of the potential dependent coverage, obtained from electrochemistry measurements, shows that the isotherm can be described by repulsive interactions using as a first approximation the Mean-Field (Frumkin) Isotherm.

Theoretical Model of Electrocompression

The electrocompression of the halide lattices can be calculated from the interfacial free energy. Here we only consider the internal energy contribution and have ignored entropic effects. This assumption is justified for the high density, hexagonal close-packed adlayers but is not correct for the low density adlayers which are not of interest here. Here we include the electrochemical potentials, $\tilde{\mu}$, and the coverage-dependent internal interaction energies of the adsorbate, $U(\theta)$. The electrical potential of the adsorbed ion is not necessarily that of the electron transferred to the metal, and this complicates the derivation below and requires some additional assumptions.

In the derivation which follows, we adopt the conventions used by Schmickler[20]. The charge of the solvated ion is ez and that of the adsorbed ion is $e(z+\lambda)$ which leaves a charge $e\lambda$ on the metal. The electrochemical potential is given by $\tilde{\mu}(\phi)$ which is related to the chemical potential, μ, the potential, ϕ, and the charge, ze. The electrochemical potential of the adsorbate is given by

$$\tilde{\mu}_{adsorbate} = \mu_{adsorbate} + e(z+\lambda)\phi_{adsorbate} \quad . \tag{1}$$

since the charge of the adsorbed ion is $e(z+\lambda)$ Finally, energy conservation requires that the electrochemical potential of the solution species must equal the sum of the electrochemical potentials of the adsorbate and that of the partial electron of charge $-e\lambda$ which is transferred. Equating theses terms yields

$$\tilde{\mu}_{solution} = \mu_{adsorbate} + e(z+\lambda)\phi_{adsorbate} - e\lambda\phi_{metal} \quad . \tag{2}$$

where ϕ_{metal} is the potential of the metal which need not correspond to that of the adsorbate. There is no known way to independently measure the potential of the adsorbate. The only potential which can be measured is that of the electron which is transferred to the metal surface, e.g. ϕ_{metal}. However, if we assume that $\phi_{adsorbate}$ is a constant fraction of ϕ_{metal}, then Eq. 2 can be simplified. With this we reformulate Eq. 2 as

$$\mu_{solution} = \mu_{adsorbate} + e\gamma\phi + e\phi_0 \tag{3}$$

where $\phi = \phi_{metal}$, γ is the electrosorption valence, and ϕ_0 is a constant. The electrosorption valence, described by Schultze and Vetter[19], is the effective charge transferred to the metal surface upon electrosorption.

The chemical potential of the of adsorbate can be expressed in terms of the derivative of the internal energy, U, with respect to the total number of adsorbed atoms, N

$$\mu_{adsorbate} = \frac{\partial U}{\partial N}|_{area} \quad . \tag{4}$$

Here U includes a sum over all of the lateral interaction energies and an energy of adsorption

$$U = U_{lateral} + U_0 \tag{5}$$

where we assume that these energies are not site specific. If U_0 is independent of the coverage the adsorption energy can be written as

$$U_0 = N u_0 \tag{6}$$

where u_0 is the adsorption energy of a single adsorbate. The lateral energy can be written as

$$U_{lateral} = \frac{1}{2} \sum_i \left[\sum_j^{i \neq j} u_{lateral}(r_{i,j}) \right] = \frac{N}{2} \sum_i u_{lateral}(r_i) \quad . \tag{7}$$

Here the double sum counts all two-particle interactions between adsorbates, independent of the separation and the factor of $1/2$ is to avoid double counting. The pairwise lateral interaction energy (discussed below) between adatoms separated by $r_{i,j}$ is $u_{lateral}(r_{i,j})$. Since we have assumed translational invariance, the double sum is reduced to a single sum where the the pairwise lateral interaction is replaced by $u_{lateral}(r_i)$. In order to relate the measured change in the nearest-neighbor separation, r, with respect to the potential, the derivative with respect to N is replaced by a derivative with respect to r through use of the relation

$$dN = -\frac{2N dr}{r} \quad . \tag{8}$$

By combining Eqs. 4-8 the chemical potential of the adsorbate is given by

$$\mu_{adsorbate} = u_0 + \left(1 - \frac{r\partial}{2\partial r}\right) \sum_i \frac{u_{lateral}(r_i)}{2} \tag{9}$$

where the first term is just the adsorption energy of a single atom and the second term is related to the lateral interactions. Given the symmetry of the adsorbate the partial derivative can be evaluated. In Eq. 9 the lateral interaction term is composed of two parts; the first is sum over all interactions for one adatom and the second is the energy to squeeze the lattice after adding an additional adatom. As we shall see below, this "squeeze" term is proportional to the radial power of the interactions.

By combining Eqs. 3 and 9, and eliminating $\mu_{adsorbate}$ the relationship between ϕ and $u_{lateral}$ emerges as

$$-e\gamma\phi - e\phi_0' = \left(1 - \frac{r\partial}{2\partial r}\right) \sum_i \frac{u_{lateral}(r_i)}{2} \tag{10}$$

where ϕ_0' is a new constant which incorporates ϕ_0, u_0, and $\mu_{solution}$. Since γ is negative for halides, increasing the potential raises the chemical potential of the adsorbate. Here the sum over all interactions (Zucker sum) can be replaced by

$$\sum_i u_{lateral}(r_i) = Z u_{lateral}(r_{nn}) \tag{11}$$

where Z is a numerical constant which estimates the number of effective nearest neighbors and $u_{lateral}(r_{nn})$ is the lateral interaction between nearest-neighbors. For a hexagonal lattice this constant is slightly larger than 6, the number of nearest-neighbors, when the lateral interactions fall rapidly with separation. This is because the interaction with non-nearest neighbors does not contribute significantly to the sum.

The lateral potential between adsorbed halides originates from the hard-core repulsion, Van der Waals attractive interactions, dipolar repulsion and substrate mediated repulsive interactions[23], often referred to as the "indirect interaction". The first two terms are grouped in the usually way to form the Lennard Jones (6/12) potential.

$$u_{LJ} = 4\epsilon' \left(\left[\frac{\sigma}{r}\right]^{12} - \left[\frac{\sigma}{r}\right]^{6} \right) \tag{12}$$

where ϵ' is the depth of the interaction well and σ is the position where $u_{LJ} = 0$. The minimum occurs at 1.12σ which is the mean spacing between adsorbates in the absence of other interactions.

Since the adsorbed halides are partially charged, presumably with an image charge on the metal side, the neighboring halides should repel each other through dipole-dipole interactions. Here it is not possible to determine the placement of the charge, rather only the dipole moment can be determined. For dipole-dipole interactions the repulsive potential is given by

$$u_{d-d} = \frac{p^2}{2\pi\epsilon_0 r^3} \tag{13}$$

where p is the dipole moment and where we have assumed that the dielectric constant is unity. The direct dipole interactions given here do not fall off as fast with distance as the induced dipole interactions, e.g the Van der Waals r^{-6} given in Eq. 12. In practice, the dipole interactions are not infinitely long range since Debye screening from the electrolyte ions provides an exponential (Yukawa type) cut-off.

In Fig. 7 we show the Cl-Cl separation versus the potential for Au(111). Note that this is the same data as shown in Fig. 4, but here the axis have been reversed for numerical convenience. We fitted the potential to the measured separation through the relationship given by Eq. 10. The solid and dashed lines represent best fits, using the potentials given by Eqs. 12 and 13. The potential offset, ϕ_0', and the dipole moment are the only adjustable parameters. We have fixed the chloride Lennard-Jones parameters to $\sigma = 3.5$Å and $\epsilon' = 13.5meV$ as reported by McDonald [21]. In the absence of other interactions, the minimum is at $1.12 \times 3.5 = 3.93$Å. This is close to, albeit slightly smaller, than the smallest Cl-Cl separation indicating that the Lennard-Jones interactions is always in the attractive regime. On the other hand, the dipolar contribution is always repulsive.

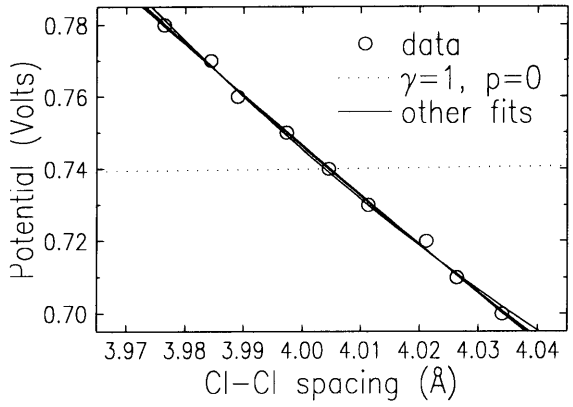

Figure 7: The measured potential versus the Cl-Cl separation for Au(111) along with various fits. Note that except for the fit with $p = 0$ (dashed line), it is difficult to distinguish the other fits (solid lines).

In the following analysis we have fitted the data with two values of γ, corresponding to complete discharge ($\gamma = -1$) and to the partial charge obtained via chronocoulometric measurements ($\gamma = -0.5$)[22]. In the latter case, the chloride still maintains half its charge when it is adsorbed.

The Cl-Cl separation can not be represented by the present formulation when $p = 0$, as indicated by the dotted line in Fig. 7 with $\gamma = -1$. The data can be equally well described by allowing the dipole moment to float in the least-squares analysis using several combinations of parameters. Fits were carried out with both values of γ and with ϵ' set to zero and the value reported by McDonald. With $\gamma = -1$, the best fit gives $p = 2.62$ D with $\epsilon' = 0$ and $p = 2.42$ D with $\epsilon' = 13.5meV$. The small difference between these two values demonstrates that the Lennard-Jones potential is not nearly large enough to describe the compression. With $\gamma = -0.5$, the best fit gives $p = 1.85$ D with $\epsilon' = 0$ and $p = 1.53$ D with $\epsilon' = 13.5meV$.

The values obtained from the analysis above are much larger than the value of 0.7 D obtained for halides on Au in UHV derived from work function measurements[24]. We note that this UHV value would give rise to a much larger electrocompression (softer lattice) than observed in our measurements. However, we remind the reader that the dipole moment derived from the electrocompression measurements is an effective value since it also includes the effect of the solution species which are not present in the vacuum. In addition, indirect interaction[23], which is mediated by the adsorbate-substrate interactions through changes in the local electronic structure, has not been incorporated in the present model. At small distances this gives rise to a repulsive interaction which scales as r^{-5}. The absence of the indirect interaction may in part describe some of the differences between the vacuum and electrochemical results.

The surface dipole moment can also been estimated from electrochemical measurements. For Cl on Au(111)[22] the dipole moment is about 0.25 D at the highest coverages, but, the exact value depends sensitively on the surface charge and reaches a minimum of 0.04 D.

The smaller value at the electrochemical interface has been attributed to screening effects from the electrolyte. Finally, we remind the reader that electrocompression measurements are sensitive to the effects of the lateral interactions whereas the dipole moments derived from the the work function and electrochemistry measurements depend only on the surface normal charge distribution.

Further analysis and data is required to fully understand the electrocompressions observed for electrodeposited adsorbates. For adsorbates on Ag(100) we are able to deduce the coverages in both the ordered and disordered phases[16]; not just in the ordered phases as is the case for adsorbates on Au(111). Here we are able to model the isotherms using a mean-field (Frumkin type) isotherm with similar values of the dipole moment as for the halides on Au(111)[16]. At the present time we do not have a complete understanding why the dipole moment, obtained from our x-ray study, UHV work function studies and electrochemical studies do not agree. A complete understanding will require a better appreciation of the indirect interaction strength and the role of solvent-adsorbate interactions.

We greatfully acknowledge the important contributions of Jia Wang to all aspect of the present work and the participation of Olaf Magnussen and Gavin Watson. The work at BNL is supported by the Division of Materials and Chemical Sciences, U.S. Department of Energy, under Contract No. DE–AC02–76CH00016. Th. Wandlowski thanks the Deutsche Forschungsgemeinshaft for support through Wa 879/2 and a Heisenberg fellowship.

References

[1] M.F. Toney, J.G. Gordon, and O.R. Melroy, SPIE Proc. **1550**, 140 (1991).

[2] M.F. Toney and O.R. Melroy, Electrochemical Interfaces: Modern Techniques for In-Situ Interface Characterization, Edited by H.D. Abruna, (VCH Verlag Chemical, Publishers, Berlin, 1991), p. 57

[3] M.F. Toney, Synchrotron Techniques in Interfacial Electrochemistry, Edited by C.A. Melendres and A. Tadjeddine, (Klewer, Dordrecht, 1994), p. 109.

[4] B.M. Ocko and J. Wang, Synchrotron Techniques in Interfacial Electrochemistry, Edited by C.A. Melendres and A. Tadjeddine, (Klewer, Dordrecht, 1994), p. 127.

[5] B.M. Ocko, O.M. Magnussen, J. X. Wang, and R.R Adžić, Nanoscale Probes of the Solid/Liquid Interface, Edited by A.A. Gewirth and H. Siegenthaler, (Klewer, Dordrecht, 1995), p. 103.

[6] A. Hamelin, and J.P. Bellier, J. Electroanal. Chem. **41**, p. 179 (1973).

[7] D.A. Scherson, and D.M. Kolb, J. Electroanal. Chem. **176**, p. 353 (1984).

[8] Gao, X.; Weaver, M. J. J. Am. Chem. Soc. **114**, p. 8544 (1992); Tao, N. J.; Lindsay, S. M. J. Phys. Chem. **96**, p. 5213 (1992).

[9] T. Yamada, K. Ogaki, S Okubu, and K. Itaya, Surf. Sci., **369**, p. 321 (1996).

[10] B.M. Ocko, G.M. Watson, and J. Wang, J. Phys. Chem. **98**, p. 897 (1994); J. Wang, G.M. Watson, and B.M. Ocko, Physica A **200**, p. 751 (1993).

[11] J. Wang, B.M. Ocko, A.J. Davenport, and H.S. Isaacs, Phys. Rev. B **46**, p. 10321 (1992).

[12] O. M. Magnussen, B.M. Ocko, J. X. Wang, and R.R. Adžić, Phys. R3v. B **51**, p. 5510 (1995).

[13] O. M. Magnussen, J. X. Wang, R.R. Adžić, and B. M. Ocko, J. Phys. Chem. **100** , p. 5500 (1996)

[14] B.M. Ocko, O.M. Magnussen, J.X. Wang, R.R Adzic, and Th. Wandlowski, Physica B **221**, p. 261 (1994).

[15] B.M. Ocko, O. M. Magnussen, J. X. Wang, and Th. Wandlowski, Phys. Rev. B **53**, p. 7654 (1996); and T. Wandlowski, J. X. Wang, O. M. Magnussen, and B. M. Ocko J. Phys. Chem. **100** , p. 10277 (1996)

[16] B.M. Ocko, J.X. Wang, Th. Wandlowski (unpublished); and Th. Wandlowski, B.M. Ocko, and J.X. Wang (unpublished)

[17] D.E. Taylor, E.D. Williams, R.L. Park, N.C. Bartelt, and T.L. Einstein, Phys. Rev. B, **32**, p. 4653 (1985).

[18] G. Valette, A. Hamelin, R. Parsons, Z. Phys. Chem. N.F. **113** p. 71 (1978).

[19] J. W. Schultze and K.J. Vetter, J. Electroanal. Chem. **44**, p. 63 (1973).

[20] W. Schmickler, **Interfacial Electrochemistry**, Oxford University Press, New York, 1996.

[21] I.R. McDonald, D.G. Bound, and M.L. Klein, Mol. Phys. **45**, p. 521 (1982).

[22] Z. Shi and J. Lipkowski, J. Electroanal. Chem. **403**, p. 225 (1996). Surf. Sci. **97** p. 409 (1980)

[23] see for instance T.L. Einstein, CRC Crit. Rev. Solid State Mat. Sci. **7**, p. 261 (1978) and T.L. Einstein and J.R. Schrieffer, Phys. Rev. B **7**, 3629 (1973).

[24] see for instance E. Bertel and F.P. Netzer, Surf. Sci. **97** p. 409 (1980)